

Swift thermal steering of domain walls in ferromagnetic MnBi stripes

Alexander Sukhov¹, Levan Chotorlishvili¹, Arthur Ernst², Xabier Zubizarreta², Sergey Ostanin², Ingrid Mertig^{1,2}, Eberhard K. U. Gross², and Jamal Berakdar^{1,*}

¹Institut für Physik, Martin-Luther-Universität, Halle-Wittenberg, D-06099 Halle/Saale, Germany

²Max Planck Institute of Microstructure Physics, D-06120 Halle/Saale, Germany

*Jamal.Berakdar@physik.uni-halle.de

ABSTRACT

We predict a fast domain wall (DW) motion induced by a thermal gradient across a nanoscopic ferromagnetic stripe of MnBi. The driving mechanism is an exchange torque fueled by magnon accumulation at the DWs. Depending on the thickness of the sample, both hot-to-cold and cold-to-hot DW motion directions are possible. The finding unveils an energy efficient way to manipulate DWs as an essential element in magnetic information processing such as racetrack memory.

Introduction

Domain walls (DWs), i.e. the cross border of regions with homogeneous but differently oriented magnetization play a central role in magnetism.¹ A particularly interesting suggestion is to exploit DWs for high density storage in a "racetrack" shift memory.^{2,3} The shifting is brought about by passing a spin-polarized current that exerts a torque on the DWs.^{4,5} While the proposal is technologically attractive it is hampered by large energy dissipation due to the high current densities needed. Recent advances resulted in an increase of the DW's velocity at lower current densities.⁶⁻⁸ It is however of interest to explore qualitatively new ways for controlling DWs. Here we show that magnonic current may serve as an efficient tool for the driving of DWs.

When a temperature gradient is applied to the system, it generates a magnon current and acts with a torque on the DWsⁱ. Strong magnetocrystalline anisotropy impedes motion of DWs. Thus, the choice of material is essential. So far, only materials with a weak magnetocrystalline anisotropy received more attention. A particular example is magnetic nanowires of permalloy ($\text{Ni}_{0.8}\text{Fe}_{0.2}$).¹⁰ Yttrium iron garnet (YIG) $\text{Y}_3\text{Fe}_2(\text{FeO}_4)_3$, $\text{Y}_3\text{Fe}_5\text{O}_{12}$ is frequently used for thermal activation of spin currents (called spin Seebeck effect SSE)¹¹⁻¹⁴ and has a slightly higher anisotropy ($K_{u1}(\text{YIG}) = -2.0 \cdot 10^3 \text{ J/m}^3$ vs. $K_{u1}(\text{permalloy}) = -1.0 \cdot 10^3 \text{ J/m}^3$).¹⁵

ⁱNo voltage bias is applied. The drift motion of the charge carriers does not affect the magnetic configuration. We note, the DWs considered here are macroscopically large on the scale of the Fermi wave length.⁹

Here we focus on manganese-bismuth compound **MnBi**, generally known as a hard ferromagnet,¹⁶ where due to a strong magnetocrystalline anisotropy the ground state possesses an out-of-plane magnetization orientation. In addition, a remarkable behavior for the temperature dependence of the magnetic anisotropy of **MnBi** was observed: Experiments and first-principles calculations reveal that the out-of-plane magnetic anisotropy in **MnBi** increases at elevated temperatures.^{17,18} As shown here, the notable temperature dependence of the anisotropy leads to a novel physical phenomena such as the acceleration of the domain wall motion. Increasing the applied temperature gradient in **MnBi** results in two distinct effects: It increases the magnonic spin current that drives the domain wall and creates gradient of the magnetocrystalline anisotropy. The width of a DW scales according to $\delta \sim \sqrt{A/K_{u1}}$. Here A is the exchange stiffness. A large magnetocrystalline anisotropy results in relatively narrow domain walls, i.e. a sharper noncollinear magnetic order and a larger exchange energy between the neighboring magnetic moments $-A\vec{M}_n\vec{M}_{n+1}$. Hence, the energy landscape forces the motion of the DW to the area of a lower magnetocrystalline anisotropy and a lower exchange energy. Thus, the temperature dependence of the magnetic anisotropy in the hard ferromagnet **MnBi** generates a fundamentally new type of spin torque, which was not studied before. The magnetocrystalline anisotropy torque acts in addition to the applied thermal bias leading to a substantial enhancement of the DW's velocity.

For a comprehensible study of the thermally activated DW motion all possible effects related to the applied thermal gradient should be addressed. An applied thermal bias generates a magnonic spin pumping current (a flux of magnons directed from the hot to the cold edge of the sample). On the path to the cold edge the magnonic current traverses the DW. Our calculations (see below) show that under certain conditions two different scenarios of the DW motion are realized: If the width of the DW is small enough (less than 7nm, see Fig.2, Fig.3 in the supplementary information) the DW is transparent for thermal magnons and the magnons pass through the DW without a sizeable change of magnons's momentum. Naturally, the spin pumping current does not exert a magnonic pressure on the DW's surface, while the angular momentum is still transferred (the angular momentum is changed by $2\hbar$ and the momentum of the magnon is conserved). A shortage of the angular momentum appears in the vicinity of the hot edge, while an extra angular momentum is accumulated at the cold edge of the sample (magnon accumulation effect, see¹⁹). In order to compensate for the imbalance in the distribution of the angular momentum, the DW propagates in the direction opposite to that of the magnon.^{20,21} As for the direction of the thermally-induced DW's motion, one should also consider the entropic torque. The free energy $F = \bar{E} - TS$ (here \bar{E} is the internal energy and S is the entropy) is minimized at elevated temperatures T . Thus, the entropic torque also provokes a motion of DW towards the hotter edge.^{22–26} One may further argue that the DW is not thermally isolated and the heat flux associated with the magnonic current influences the entropy of the DW.²⁷ However, the influence of the entropic torque on the DW motion is an established trend with the DW moving towards the hot edge.

For a DW width exceeding 15nm, the magnonic spin pumping current is totally reflected by the DW. Therefore, in this case a second scenario is relevant: The magnons exert a sustainable pressure on the DW's surface. If the magnonic pressure is strong enough, a thermally activated spin pumping current drags the DW to the cold edge. Our full numerical calculations evidence that indeed the direction of the DWs motion is system dependent. The microscopic theory²⁸ predicts a strong magnonic recoil

effect for the DW motion. The momentum of the DW depends on the tilt angle of its plane. If a magnon is reflected by the DW, the conservation of the total angular momentum induces a rotation of the DW. Thus, the magnon reflection leads to a motion of the DW in the direction of magnonic current.^{28,29} The pressure exerted by the magnonic current on the DW reads: $P = 2\delta n v_k \hbar k$. Here $v_k = |\vec{v}_k|$, $k = |\vec{k}|$ are the velocity and the wave vector of magnons, $\delta n = n_{neq}(T) - n_{eq}(T)$ quantifies the magnon accumulation effect, i.e. the excess of the density of non-equilibrium magnons $n_{neq}(T)$ compared to the reference number of equilibrium magnons $n_{eq}(T)$ at the same temperature, but in the absence of the thermal gradient. Exerted pressure is proportional to the applied thermal bias. Our calculations (see Fig. 1 of Suppl. Information) are in line with the fact that magnons created in the hot area propagate toward the cold area. The left (right) side of the DW's (see Fig. 1) is associated with the high (low) temperature of the applied thermal gradient. Therefore, the magnon accumulation is positive $\delta n > 0$ at the left side of the DWs and is negative $\delta n < 0$ at the right side exerting a magnonic pressure that drives the DWs. The direction of the motion of DW depends considerably on the ratio between the reflected and the transmitted magnons. The velocity of the DW can then be evaluated according to³⁰

$$V_{DW} = -\frac{R}{1+\alpha^2}U + \frac{\alpha(1-R)\Delta k}{1+\alpha^2}U. \quad (1)$$

Here $U = (\gamma \hbar n v_k) / (\mu_B M_s)$, α is the phenomenological Gilbert damping, γ is the gyromagnetic ratio, M_s is the saturation magnetization, Δ is the width of the DW and k is the magnon's wave vector, and $0 < R < 1$ is the transmission coefficient. Driving DW via the spin waves excited by a microwave field shows a strong frequency dependence.²⁰ In contrast to the field-driven DW motion,³¹ the thermally activated magnonic spin current is non-monochromatic.³² Spectral characteristics of the magnons contributing to the magnonic accumulation are not yet fully settled. The magnonic current could be due to the difference between the magnon and the phonon temperatures.³³ Recent spatially resolved experiments carried out via Brillouin light scattering technique³⁴ show a non-vanishing spin current for equal magnon and phonon temperatures. However, as shown in,³⁵ the thermally activated spin current is dictated by the magnon temperature profile rather than by the difference between the phonon and the magnon temperatures. In a recent experiment³⁶ low frequency subthermal magnons were identified as a source for the spin current. These are magnons with a frequency lower than the internal cutoff frequency $\omega = \gamma \left(H_{\text{eff}} + \frac{2A}{M_s} k^2 \right) < \omega_c$ (here A is the exchange stiffness and H_{eff} stands for the effective magnetic field). The internal cutoff frequency is not related to the structure of the DW but to the spectrum of the thermally excited magnons. The frequency spectrum of the thermally excited magnons is not monochromatic and covers a certain frequency domain. The internal cutoff frequency ω_c is the highest frequency of the magnons, which are excited thermally. Hence, the magnons with frequencies higher than the internal cutoff frequency $\omega > \omega_c$ do not contribute to the thermally activated magnonic current.^{36,37} We observed that magnons can either pass through the DW or are reflected off the DW depending on the geometry (thickness) of DW itself, while the spectral characteristics of the magnons (defined by thermal bias) are irrelevant. We find that in the case of a non-monochromatic, thermally activated magnonic current the ratio between the reflected and the transmitted magnons depends crucially on the characteristics of the DW itself, rather than on the cutoff frequency ω_c . For the same magnonic current we detect DWs with

different geometry moving in the opposite direction.

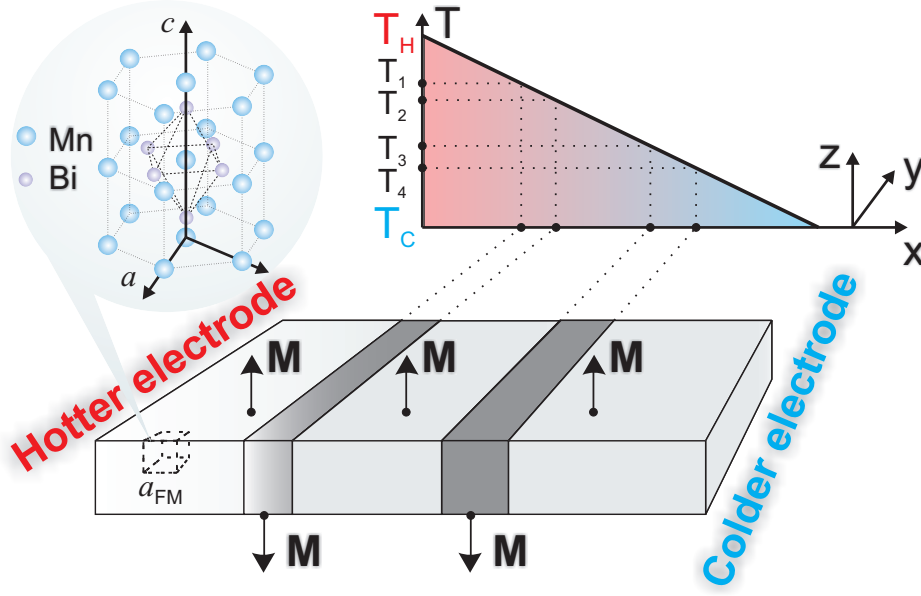


Figure 1. Schematics of the considered structure with a thermal bias applied along the x-axis. \vec{M} indicates the direction of the magnetization within a domain, $a_{\text{FM}} = 1 \text{ nm}$ represents the coarse-grained FM cell including the average over several MnBi unit cells, whose crystallographic c -axis coincides with the z -axis.

Results

As shown in Figs. 2, a)-d), a homogeneously heated sample does not lead to a directed domain wall motion in the sample, but rather a redistribution of domains on a long time scale is observed. Considering the time laps of [10 : 500] ns while a linear temperature gradient is applied and accounting also for the temperature dependence for the magnetocrystalline anisotropy¹⁸ (the anisotropy is stronger for higher temperatures), we observe (cf. Fig. 2, e)-h)) that almost all domains reach the right edge of the sample. Also the size of FM domains is reduced during their motion. The pressure exerted by the magnon accumulation effect modifies the shape of DWs. Fig. 3 illustrates the domain wall motion. The averaged velocity of the domain wall motion $\langle V_{\text{DW}} \rangle$ is plotted as a function of the linear temperature gradient. As expected, the velocity grows with elevating the temperature gradient, however it shows a slight saturation at higher gradients. The reason for that is the saturation of the magnonic current which was theoretically predicted in Ref.³⁸ Surprisingly, the demagnetizing fields do not influence much the domain wall speed for a homogeneous anisotropy (Fig. 3, circles and squares). The inhomogeneity of the anisotropy induced by the temperature gradient increases the speed of domain wall motion by approximately one order of magnitude.

Our general interpretation of the obtained DW dynamics relies on the definition of the magnon spin current given in Ref.³⁵ by a recursive formulaⁱⁱ. The x-component of the spin current $I_x^{M_{x,y,z}}(t)$ is calculated in a time-resolved manner. Fig. 4 demonstrates clearly that most crucial for the magnon spin current is the presence of FM domain walls, where different

ⁱⁱRecursive relation for the spin current: $I_n^\alpha = I_0^\alpha - \frac{2Aa}{M_S^2} \sum_{m=1}^n M_m^\beta (M_{m-1}^\gamma + M_{m+1}^\gamma) \varepsilon_{\alpha\beta\gamma}$, where $\varepsilon_{\alpha\beta\gamma}$ is the Levi-Civita antisymmetric tensor, A effective exchange stiffness, a lattice constant, and M_S saturation magnetization. Greek indexes define the current components and the Latin ones denote sites.

components of the magnon-current tensor show pronounced peaks. The accumulation of the magnon spin current at the domain walls leads to a torque acting on the domain walls, shifting them towards the colder edge. The situation might be different if the thickness of the sample is drastically reduced. In this case the magnonic spin current penetrates the DWs (Fig. 5) and the entire domain walls move towards the hotter electrode. However in this case the DWs move opposite to the anisotropy gradient. Therefore, the velocity of the DWs decreases.

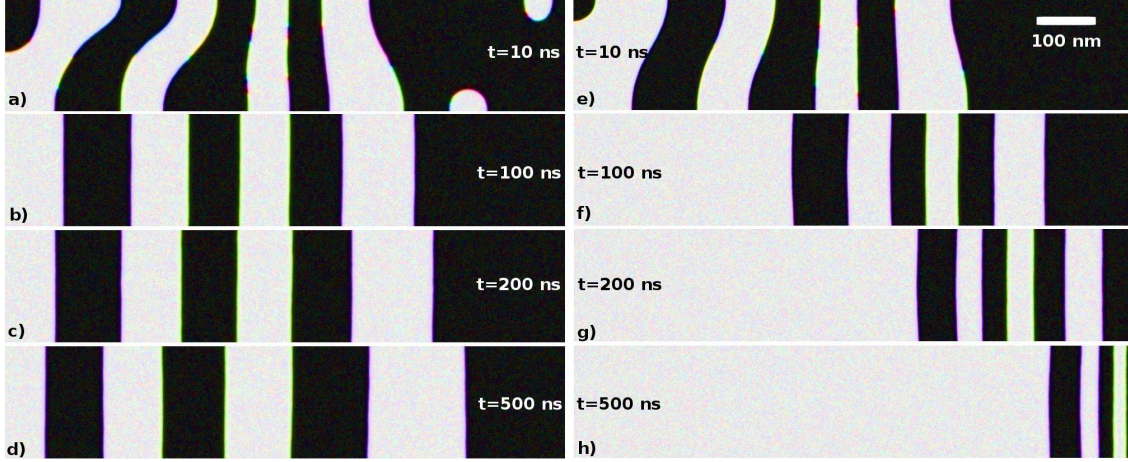


Figure 2. Top view of the magnetization configuration with no temperature gradient applied $\nabla_x T = 0$ (left panel, a-d) and the magnetization configuration for both $\nabla_x T = 0.15$ K/nm and $K_{ul}(T) = (9.69 \cdot 10^3 T - 1.12 \cdot 10^6)$ J/m³ (right panel, e-h) of a 1000nm×200nm×25nm MnBi sample at $T_C = 300$ K and different time moments in the range [0 : 500] ns. The light color represents the magnetization pointed towards the reader and the dark color indicates the magnetization away from the reader both perpendicularly to the surface of the figure (cf. Fig. 1). The magnetization configuration is calculated including long-range interactions (the demagnetizing fields). The anisotropy strength is set according to first-principles calculations of Ref.¹⁸ fitted for the interval of [300 : 400] K (right panel, e-h). A thermal bias is applied to the sample such that $T_H - T_C = 150$ K. All simulations were performed with the initial state at $t = 0$ being always chosen randomly with regard to the magnetization orientation. Then, the magnetization of a given sample was relaxed up to 10ns in the absence of an external thermal bias.

Discussion

We studied thermally activated motion of the DWs in the manganese-bismuth compound MnBi, generally known as a hard ferromagnet. We found that the unusual dependence of the magnetocrystalline anisotropy on the temperature (magnetocrystalline anisotropy in MnBi increases at elevated temperatures) is advantageous for a fast thermal steering of DWs. Sharp noncollinear magnetic orders formed under the strong magnetocrystalline anisotropy are energetically unfavorable. Therefore, the DWs slip to areas of small magnetocrystalline anisotropy. Thus, the gradient of the magnetocrystalline anisotropy acts as a macroscopic

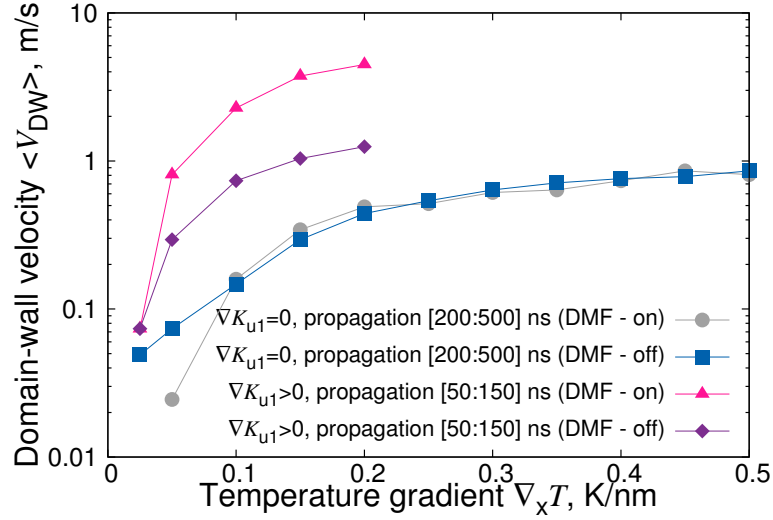


Figure 3. Dependence of the average domain-wall velocity on the temperature gradient $\nabla_x T$ for a 1000nm×200nm×25nm MnBi sample. The parameters are taken from Table 1 (Supplem. Information) and for $\alpha = 1.0$. "DMF" stands for demagnetizing fields which are taken (or not) into account for the respective curves. Solid circles and squares represent the data for zero anisotropy gradient ∇K . Triangles and diamonds show the situation with non-zero anisotropy gradient according to the first-principles calculations of Ref.¹⁸ fitted for the interval of [300 : 400] K as $K_{u1}(T) = (9.69 \cdot 10^3 T - 1.12 \cdot 10^6) \text{ J/m}^3$. The increase of the DW's velocity is a cooperative effect of the anisotropy gradient and the demagnetization fields. When the magnetocrystalline anisotropy gradient is applied the demagnetization field contributes to the formation of domains. We observed (not shown) that domains in this case are smaller and this enhances their mobility.

driving assisting the thermally activated motion of the DWs. The microscopic mechanism for the DWs motion is based on the magnonic spin current. The reflected magnonic spin current drags the DW to the cold edge while transmitted current forces the DW to the hot edge. We also observe a deformation of the shape of DWs due to the pressure exerted by the accumulation of magnons.

Methods

To provide parameters for our model simulations we performed extensive first-principles study of MnBi using a self-consistent Green function method within the framework of the density functional theory.³⁹ The ground state properties were calculated for the experimental lattice constant, while for the magnetic anisotropy energy (MAE) calculations the crystalline structure parameters were adopted from experiments, which studied the dependence of the MAE on the applied temperature.¹⁷ First of all, we found that our simulations within the generalized gradient approximation provide an adequate description of MnBi. The main ground state properties, obtained within our calculations, are listed in the Table 1, second column (Supplem. Information). Thus, in accordance with experiments, MnBi is a robust ferromagnet with Curie temperature of 680 K. The magnetic moments and exchange interaction parameters, estimated within the magnetic force theorem, provide the exchange stiffness close to the

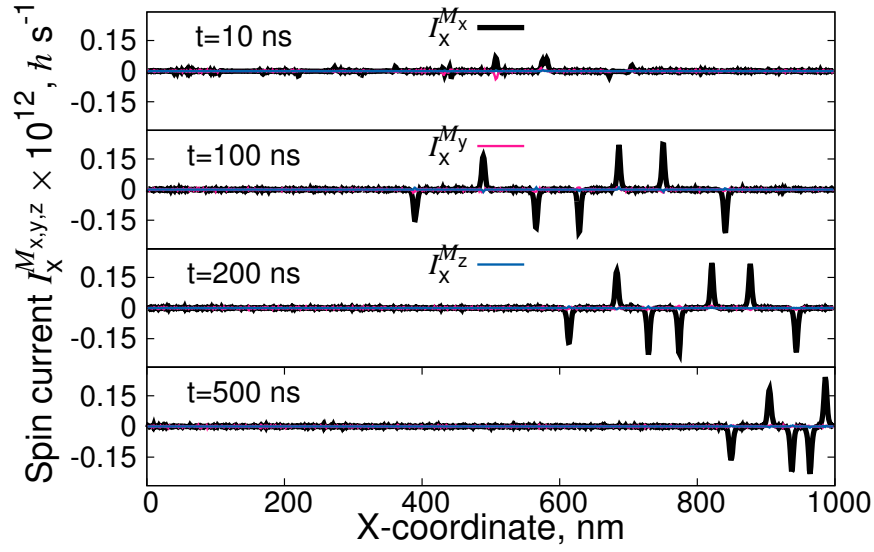


Figure 4. Time-resolved magnon spin currents corresponding to magnetic configurations shown in Fig. 2 (right panel) of a $1000\text{nm} \times 200\text{nm} \times 25\text{nm}$ MnBi sample for the temperature gradient of 0.15 K/nm at different times in the range $[0 : 500] \text{ ns}$. The left side of the sample is hotter, the right edge is always kept at room temperature. The magnetization configuration is calculated for *non-zero* demagnetizing fields. Anisotropy gradient is chosen according to first-principles calculations of Ref.¹⁸ fitted for the interval of $[300 : 400] \text{ K}$ in the form $K_{u1}(T) = (9.69 \cdot 10^3 T - 1.12 \cdot 10^6) \text{ J/m}^3$.

experimental values (cf. Table 1 (Supplem. Information)). The MAE calculated for $T = 0 \text{ K}$ and for higher temperatures is in a good agreement with the experimental results and other theoretical studies.^{17, 18} The influence of the conductance electrons is incorporated in the effective exchange stiffness.⁴⁰

With the microscopic parameters delivered by experiments and first principles calculations we performed micromagnetic simulation for the magnetization dynamics on the basis of Landau-Lifshitz-Gilbert (LLG) equation, as implemented in the mumax3-micromagnetic simulation package.⁴¹

Supplementary Information

Table 1 gives an overview over the main parameters that are relevant for the magnetic MnBi-alloy. In the present calculations the parameters termed as "experimental values" (third column) were employed. One of the main parameter that is important for the magnetic configuration is the ferromagnetic (FM) cell a_{FM} . It should be chosen such that detailed magnetic structures such as FM domains can be resolved. It is known¹⁵ that the width of FM domain walls scales according to $\delta \sim \sqrt{A/K_{u1}}$, where A is the exchange stiffness. Since the magneto crystalline anisotropy K_{u1} in MnBi is very high, it results in a relatively narrow domain walls with widths around $2 - 6 \text{ nm}$. To resolve fine structures within the domain walls we deemed, upon tests, that

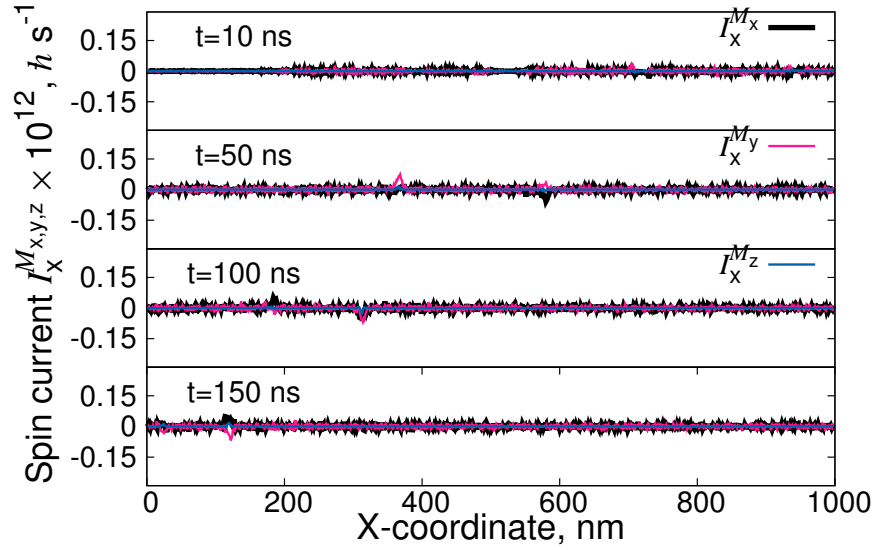


Figure 5. Time-resolved magnon spin currents of a 1000nm×200nm×1nm MnBi sample for the temperature gradient of 0.15 K/nm at different times in the range [0 : 150] ns. The left side of the sample is hotter, the right edge is always kept at room temperature. The magnetization configuration is calculated for *non-zero* demagnetizing fields. The anisotropy is homogeneous, i.e. $K_{u1} = 1.75 \cdot 10^6$ J/m³.

$a_{\text{FM}} = 1$ nm as appropriate. In the *ab-initio*-calculations we obtained the value for the saturation magnetizationⁱⁱⁱ and the exchange stiffness constant^{iv} shown in Table 1. For comparison, analogous values for the exchange stiffness^v, the Gilbert damping^{vi} and the FM cell size^{vii} are also listed in Table 1.

The size of the simulated MnBi sample has the dimension of 1000 nm along the x-axis, 200 nm along the y-axis, and a thickness of 25 nm (Sections I, II and III). It required 1.2 GB of the GPU-memory while including demagnetizing fields. To examine the dynamics of domain walls we focused on an stripe sample with the temperature gradient being along the stripe (chosen as the x-direction). The value 25 ÷ 30 nm for the sample thickness was taken in accordance with the minimal known thickness where a magnetic pattern was still recognizable.⁴²

In order to initiate FM domains, we proceed in a natural way by starting from a random magnetic configuration at zero magnetic field and at room temperature ($T = 300$ K). To achieve convergence to a well-defined magnetic configuration a relatively large damping was chosen which resulted in a convergence to the ground state on the time scale of several to ten nanoseconds (simulation time step was set to $5 \cdot 10^{-13}$ s). After reaching the ground state which is a magnetic pattern with

ⁱⁱⁱCalculated as $M_S = \frac{\mu_S}{V_0}$, where $V_0 = 137.48 \text{ \AA}^3$ is a volume of the unit cell and $\mu_S(T = 0\text{K}) = 8.4\mu_B$ or $\mu_S(T = 300\text{K}) = 7.33\mu_B$ for MnBi.

^{iv}Calculated based on the ratio $A = \frac{DM_S}{2g\mu_B}$ (in MnBi $D = 670 \text{ meV \AA}^2$), which is derived in Ref.⁴⁴

^vCalculated from the ratio for the FM domain wall thickness $\delta_{\text{FM}} = \sqrt{A/K_{u1}}$ based on values from Ref.⁴³ at room temperature.

^{vi}Calculated based on the ratio $\alpha = \frac{\sqrt{3}}{2} \frac{\gamma}{\omega} \Delta B_{\text{pp}}$, which is approximated for the half-height of the width of the FMR spectrum curve at $T = 130$ K. The values of $\Delta B_{\text{pp}} \approx 0.05$ T, $\omega/(2\pi) = 9$ GHz are taken from Ref.⁴⁵ Gyromagnetic ratio is $\gamma = 1.76 \cdot 10^{11} (\text{Ts})^{-1}$.

^{vii}Should be of the order of 2.5 nm, which is min. δ_{FM} ($T=300$ K) based on values of Ref.⁴³

several FM domain walls (typically after 10 ns), the temperature gradient is applied, where the hotter end is the left part of the sample, whereas the right end is always kept at room temperature.

The magnetic configurations with time are obtained from the solution of the Landau-Lifshitz-Gilbert (LLG) equation within the micromagnetic framework by means of `mumax3`-software.⁴¹

DESCRIPTION	<i>ab-initio</i>	EXPERIMENT
Magnetization M_S , [A/m]	$5.6 \cdot 10^5$ ($T = 0$ K) $4.9 \cdot 10^5$ ($T = 300$ K)	$7.42 \cdot 10^5$ ($T=0$ K) ⁴³ $6.40 \cdot 10^5$ ($T=300$ K) ⁴³
Exch. stiffness A , [J/m]	$1.43 \cdot 10^{-11}$	$6.25 \cdot 10^{-12}$
Anis. strength $K_{ul}(T)$, [J/m ³]	$-0.44 \cdot 10^6$ ($T = 0$ K)? $1.4 \cdot 10^6$ ($T = 300$ K)?	$1.75 \cdot 10^6$ ($T = 300$ K) ⁴³
Anisotropy type	uniaxial	uniaxial
Gilbert damping α	-	0.0054 ($T=130$ K)
Curie-Temperature T_C , [K]	680	775 (Ref. ⁴³)
FM cell size a_{FM} , [nm]	-	2.5

Table 1. Parameters relevant for MnBi-alloy.

Domain-wall motion

Fig. 6 provides additional illustration of the DW motion under thermal bias.

Domain-wall thickness

In Figs. 7, 8 we demonstrate the trend in the thermally assisted DW motion with the DW thickness.

References

1. Hubert, A. & Schäfer, R. *Magnetic Domains* (Springer-Verlag, Berlin, 1998).
2. Hayashi, M., Thomas, L., Moriya, R., Rettner, Ch. & Parkin, S.S.P. Current-Controlled Magnetic Domain-Wall Nanowire Shift Register. *Science* **320**, 209 (2008).
3. Parkin, S. S. P., Hayashi, M. & Thomas, L. Magnetic Domain-Wall Racetrack Memory. *Science* **320**, 190 (2008).
4. Berger, L. Emission of spin waves by a magnetic multilayer traversed by a current. *Phys. Rev. B* **54**, 9353 (1996).
5. Slonczewski, J. C. Current-driven excitation of magnetic multilayers. *J. Magn. Magn. Mater.* **159**, L1 (1996).

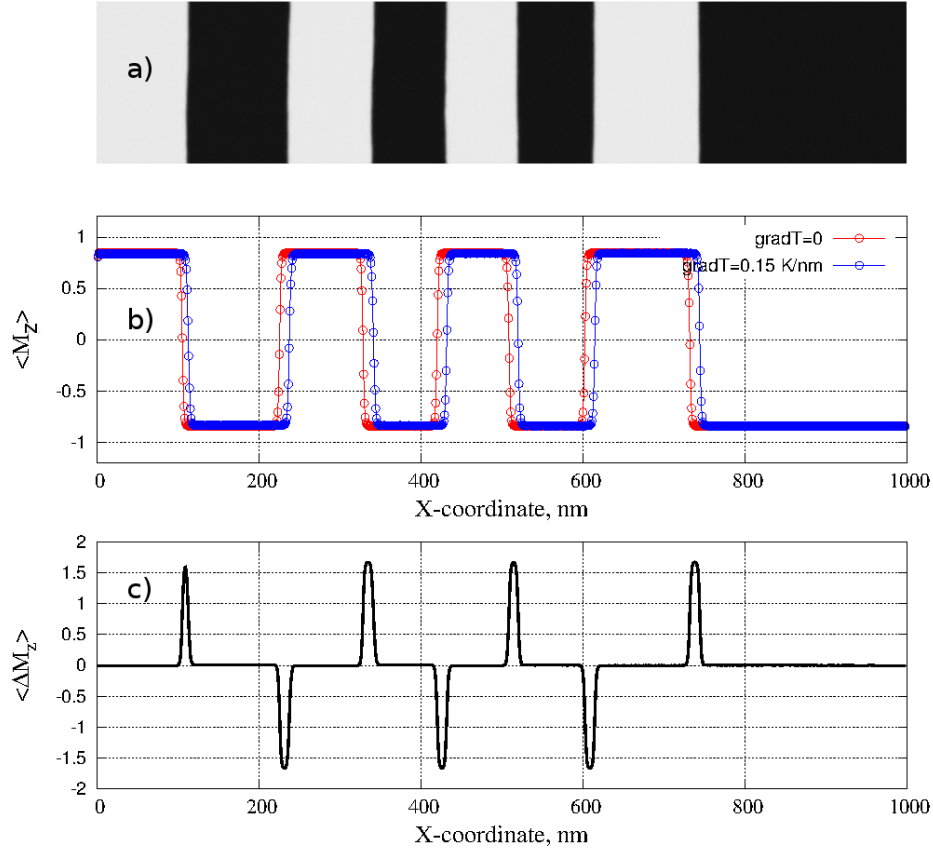


Figure 6. (a) Top view of the magnetization configuration (black color indicates the magnetization direction "down", white color implies the magnetization direction "up") of a 1000nm×200nm×25nm MnBi sample for the temperature gradient of 0.15 K/nm at time 100 ns. The spin accumulation (c) is calculated according to the expression $\langle \Delta M_z^n \rangle = \langle M_z^n \rangle|_{\nabla T \neq 0} - \langle M_z^n \rangle|_{\nabla T = 0}$ for a 1000nm×200nm×25nm MnBi sample, where $\langle M_z^n \rangle|_{\nabla T = 0}$ (b) stands for the data with no temperature gradient at time $t = 100$ ns and $\langle M_z^n \rangle|_{\nabla T \neq 0}$ (b) is for the data with a temperature gradient 0.15 K/nm at time $t = 100$ ns. (c) A positive spin accumulation corresponds always to the left side of domains, negative values of the spin accumulation are associated with the right side of the corresponding domains.

6. Phung, T. et al. Highly Efficient In-Line Magnetic Domain Wall Injector. *Nanoletters* **15**, 835 (2015).
7. Yang, S.-H., Ryu, K.-S. & Parkin, S. S. P. Domain-wall velocities of up to 750 m s⁻¹ driven by exchange-coupling torque in synthetic antiferromagnets. *Nature Nanotechnology* **10**, 221 (2015).
8. Parkin, S. S. P. & Yang, S.-H. Memory on the racetrack. *Nature Nanotechnology* **10**, 195 (2015).
9. Tatara, G., Kohno, H., & Shibata, J. Microscopic approach to current-driven domain wall dynamics. *Phys. Rep.* **468**, 213 (2008).
10. Thomas, L. et al. Oscillatory dependence of current-driven magnetic domain wall motion on current pulse length. *Nature* **443**, 197 (2006).
11. Kirihaara, A. et al. Spin-current-driven thermoelectric coating. *Nature Materials* **11**, 686 (2012).

12. Uchida, K. et al. Observation of the spin Seebeck effect. *Nature* **455**, 778 (2008).
13. Jaworski, C. M. et al. Observation of the spin-Seebeck effect in a ferromagnetic semiconductor. *Nature Materials* **9**, 898 (2010).
14. Uchida, K. et al. Spin Seebeck insulator. *Nature Materials* **9**, 894 (2010).
15. Coey, J. M. D. *Magnetism and Magnetic Materials* (Cambridge University Press, New York, 2010).
16. Coey, J. M. D. New permanent magnets; manganese compounds. *J. Phys.: Condens. Matter* **26**, 064211 (2014).
17. Stutius, W. E., Chen, T., & Sandin, T. R. Magnetism and Magnetic Materials. *AIP Conf. Proc.* **18**, 1222 (1974).
18. Antropov, V. P., Antonov, A. N., Bekenov, L. V., Kutepov, A., & Kotliar, G. Magnetic anisotropic effects and electronic correlations in MnBi ferromagnet. *Phys. Rev. B* **90**, 054404 (2014).
19. Ritzmann, U., Hinzke, D. and Nowak U. Propagation of thermally induced magnonic spin currents *Phys. Rev. B* **89**, 024409 (2014).
20. Yan, P., Wang, X. S., & Wang, X. R. All-Magnonic Spin-Transfer Torque and Domain Wall Propagation. *Phys. Rev. Lett.* **107**, 177207 (2011).
21. Tatara, G. & Kohno, H. Theory of Current-Driven Domain Wall Motion: Spin Transfer versus Momentum Transfer. *Phys. Rev. Lett.* **92**, 086601 (2004).
22. Hinzke, D & Nowak, U. Domain Wall Motion by the Magnonic Spin Seebeck Effect. *Phys. Rev. Lett.* **107**, 027205 (2011).
23. Schlickeiser, F., Ritzmann, U., Hinzke, D., & Nowak, U. Role of Entropy in Domain Wall Motion in Thermal Gradients. *Phys. Rev. Lett.* **113**, 097201 (2014).
24. Wang, X. S. & Wang, X. R. Thermodynamic theory for thermal-gradient-driven domain-wall motion. *Phys. Rev. B* **90**, 014414 (2014).
25. Kovalev, A. A. & Tserkovnyak, Y. Thermomagnonic spin transfer and Peltier effects in insulating magnets. *Europhys. Lett.* **97**, 67002 (2012).
26. Jiang, W. et al. Direct Imaging of Thermally Driven Domain Wall Motion in Magnetic Insulators. *Phys. Rev. Lett.* **110**, 177202 (2013).
27. Yan, P., Cao, Y., & Sinova, J. Thermodynamic Magnon Recoil for Domain Wall Motion. *Phys. Rev. B* **92**, 100408(R) (2015).
28. Yan, P., Kamra, A., Cao, Y., & Bauer, G. E. W. Angular and linear momentum of excited ferromagnets. *Phys. Rev. B* **88**, 144413 (2013).
29. Yan, P. & Bauer, G. E. W. Magnonic Domain Wall Heat Conductance in Ferromagnetic Wires, *Phys. Rev. Lett.* **109**, 087202 (2012).

30. Wang, X.-G., Guo, G.-H., Nie, Y.-Zh., Zhang, G.-F., & Li, Z.-X. Domain wall motion induced by the magnonic spin current. *Phys. Rev. B* **86**, 054445 (2012).
31. Wang, X. S., Yan, P. Shen, Y. H., Bauer, G. E. W. and Wang, X. R. Domain Wall Propagation through Spin Wave Emission. *Phys. Rev. Lett.* **109**, 167209 (2012).
32. Chotorlishvili, L., Etesami, S.R., Berakdar, J., Khomeriki, R., and Ren, J. Electromagnetically controlled multiferroic thermal diode. *Phys. Rev. B* **92**, 134424 (2015).
33. Xiao, J., Bauer, G. E. W., Uchida, K.-C., Saitoh, E., & Maekawa, S. Theory of magnon-driven spin Seebeck effect. *Phys. Rev. B* **81**, 214418 (2010).
34. Agrawal, M. et al. Direct Measurement of Magnon Temperature: New Insight into Magnon-Phonon Coupling in Magnetic Insulators. *Phys. Rev. Lett.* **111**, 107204 (2013).
35. Etesami, S. R., Chotorlishvili, L., Sukhov, A. & Berakdar, J. Longitudinal spin current induced by a temperature gradient in a ferromagnetic insulator. *Phys. Rev. B* **90**, 014410 (2014).
36. Boona, S. R. & Heremans, J.P. Magnon thermal mean free path in yttrium iron garnet. *Phys. Rev. B* **90**, 064421 (2014).
37. Etesami, S. R., Chotorlishvili, L., and Berakdar, J. Spectral characteristics of time resolved magnonic spin Seebeck effect *Appl. Phys. Lett.* **107**, 132402 (2015).
38. Chotorlishvili, L. et al. Fokker-Planck approach to the theory of the magnon-driven spin Seebeck effect. *Phys. Rev. B* **88**, 144429 (2013).
39. Lüders, M., Ernst, A., Temmerman, W. M., Szotek, Z., Durham, P. J. Ab initio angle-resolved photoemission in multiple-scattering formulation. *J. Phys.: Cond. Matter* **13**, 8587 (2001).
40. Liechtenstein, A. I., Katsnelson, M. I., Antropov, V. P. & Gubanov, V. A. Local spin density functional approach to the theory of exchange interactions in ferromagnetic metals and alloys. *J. Magn. Magn. Mater.* **67**, 65 (1987).
41. Vansteenkiste, A. et al. The design and verification of MuMax3. *AIP Advances* **4**, 107133 (2014).
42. Dekker, P. *Magnetization reversal processes in thin MnBi films* (Dissertation, bibliothek TU Delft, 1974).
43. Guo, X., Chen, X., Altounian, Z., & Ström-Olsen, J. O. Magnetic properties of MnBi prepared by rapid solidification. *Phys. Rev. B* **46**, 14578 (1992).
44. Hamrle, J. et al. Determination of exchange constants of Heusler compounds by Brillouin light scattering spectroscopy: application to Co₂MnSi. *J. Phys. D: Appl. Phys.* **42**, 084005 (2009).
45. Chen, D., Gondo, Y. Temperature Dependence of the Magneto-Optic Effect and Resonance Phenomena in Oriented MnBi Films. *J. Appl. Phys.* **35**, 1024 (1964).

Acknowledgements

This work is supported by the Deutsche Forschungsgemeinschaft under grants BE 2161/5-1, ER 340/5-2, ME 1153/15-2 and by the Joint Initiative for Research and Innovation within the Fraunhofer and Max Planck cooperation program.

Author contributions statement

All authors contributed to the discussion and analysis of the research. A. S. performed micromagnetic simulations, L. C. and J. B. provided the theoretical explanation and compiled the text. A. E, X. Z., S. O., I. M., E. K. U. G. performed DFT calculations and provided parameters for the model.

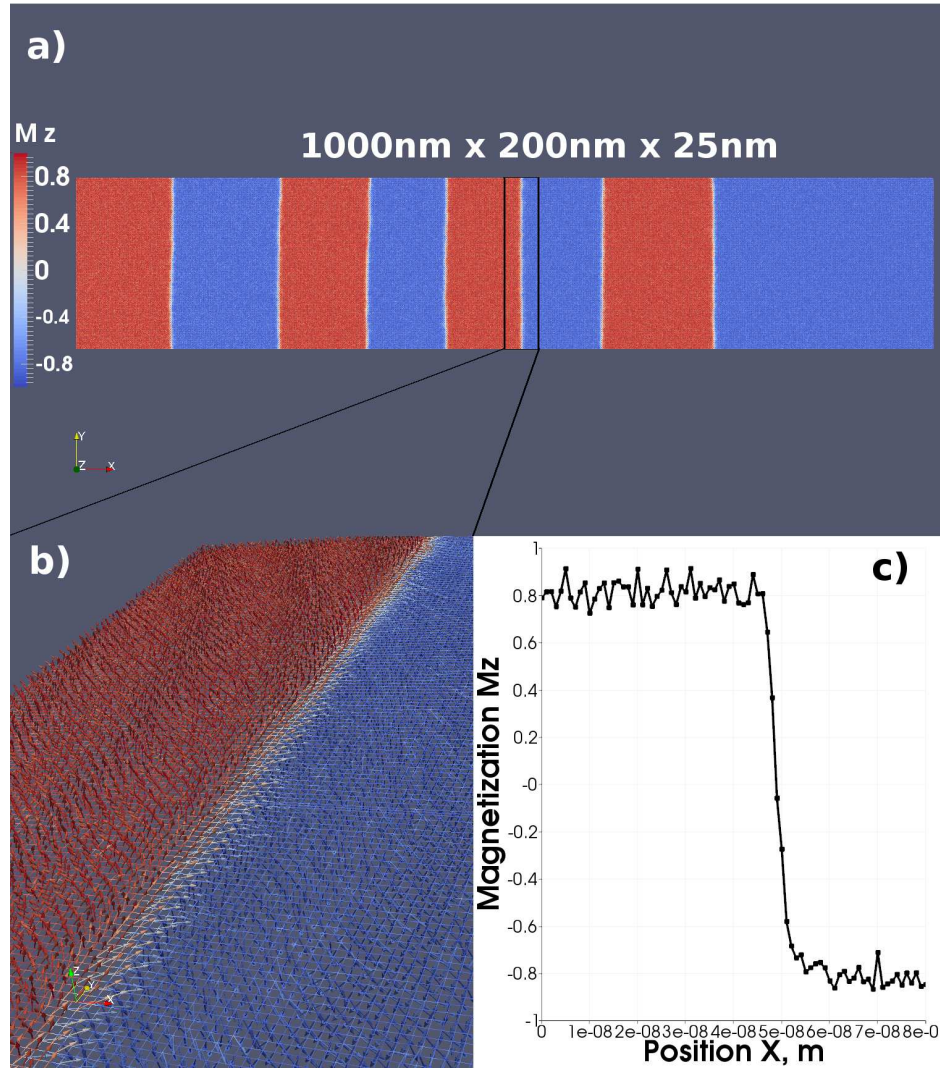


Figure 7. (a) Top view of the magnetization configuration (blue color indicates the magnetization direction "down", red color implies the magnetization direction "up") of a 1000nm×200nm×25nm MnBi sample for the temperature gradient of 0.15 K/nm at time 100 ns ($\nabla K_{ul} = 0$, DMF - on). (b) stands for the magnetization configuration frame between [470 : 570] nm (top layer only). (c) indicates the averaged magnetization profile along a line drawn parallel to the x-direction and connecting edges of the frame [470 : 570] nm for the top layer. The resulting domain-wall thickness is $d_{DW} \approx 15$ nm.

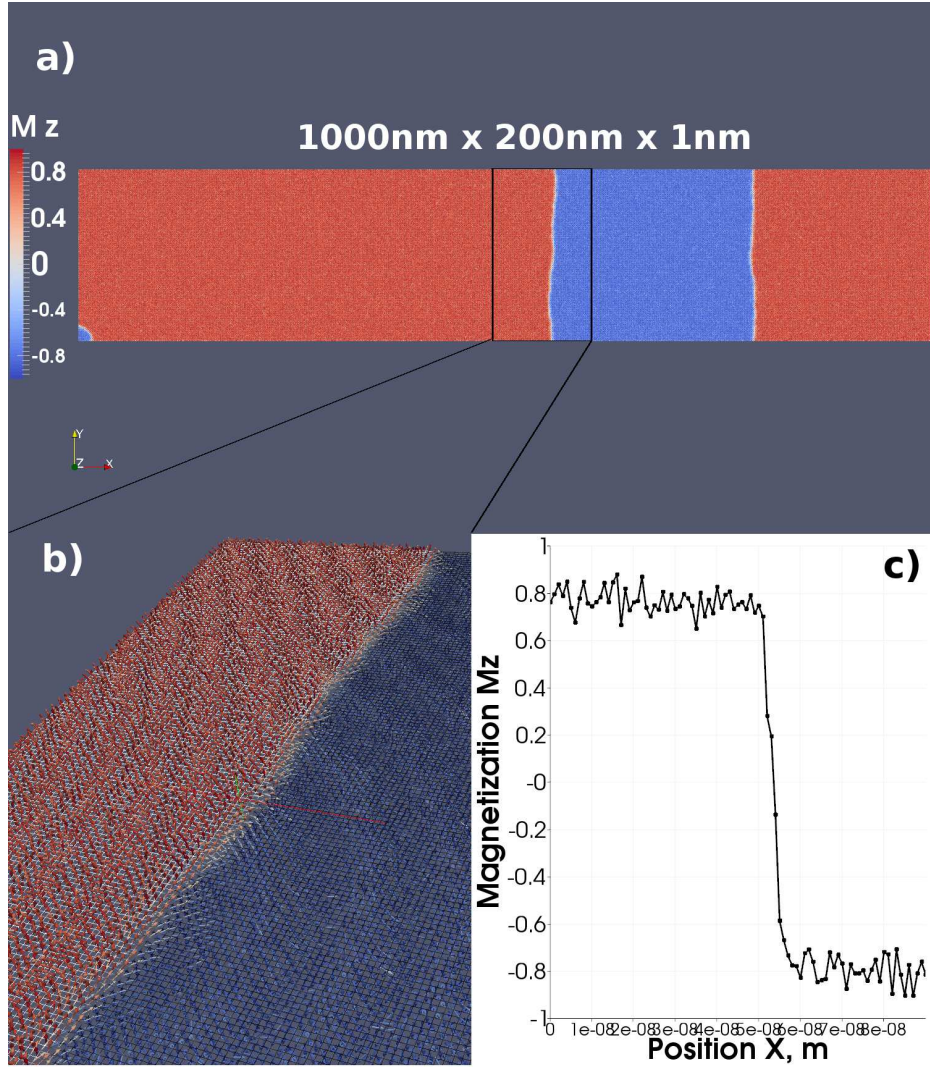


Figure 8. Same as in Fig. 7 but (a) for the temperature gradient of 0.15 K/nm at time 20 ns ($\nabla K_{ul} = 0$, DMF - on). (b) the magnetization configuration frame is between [500 : 600] nm. (c) the averaged magnetization profile for the frame [500 : 600] nm. The resulting domain-wall thickness is $d_{DW} \approx 7$ nm.